TITLE PAGE

Age-Modulated Immuno-Metabolic Proteome Profiles of Deceased Donor Kidneys Predict 12-Month Posttransplant Outcome

Authors: Philip D Charles[1,2†], Sarah Fawaz[3,4*], Rebecca H Vaughan[3,4*], Simon Davis[2], Priyanka Joshi[3], Iolanda Vendrell[2], Ka Ho Tam[5], Roman Fischer[2], Benedikt M Kessler[2], Edward J Sharples[6], Alberto Santos[1,7,8], Rutger J Ploeg[3,4], Maria Kaisar[3,4†]

Affiliations:

[1]Big Data Institute, Nuffield Department of Medicine, University of Oxford; Oxford, United Kingdom.

[2]Target Discovery Institute, Centre for Medicines Discovery, Nuffield Department of Medicine, University of Oxford; Oxford, United Kingdom.

[3]Research and Development, NHS Blood and Transplant; Bristol & Oxford, United Kingdom.

[4]Nuffield Department of Surgical Sciences and Oxford Biomedical Research Centre, University of Oxford; Oxford, United Kingdom.

[5]Engineering Department, University of Oxford; United Kingdom.

[6]University Hospital Oxford; Oxford, United Kingdom.

[7]Center for Health Data Science, University of Copenhagen; Copenhagen, Denmark.

[8]Novo Nordisk Foundation Center for Protein Research, University of Copenhagen; Copenhagen, Denmark.

*These authors contributed equally.

†Corresponding authors. Email: philip.charles@ndm.ox.ac.uk; maria.kaisar@nds.ox.ac.uk

Keywords:

Kidney transplantation, Machine Learning, Data Independent Acquisition, Proteomics, Donor Age, QUOD

ABSTRACT

Background. Organ availability limits kidney transplantation, the best treatment for end-stage kidney disease. Deceased donor acceptance criteria have been relaxed to include older donors with higher risk of inferior posttransplant outcomes. Donor age, although significantly correlates with transplant outcomes, lacks granularity in predicting graft dysfunction. Better characterization of the biological mechanisms associated with deceased donor organ damage and specifically predictive of transplant outcome in recipients is key to developing new assessment criteria for donor kidneys and developing function-preserving interventions.

Methods. 185 deceased donor pretransplant biopsies with clinical and demographic donor and recipient metadata were obtained from the Quality in Organ Donation biobank (QUOD), selected on the basis of 12-month paired posttransplant function and deep proteomic profiles acquired by mass spectrometry. Using a $2/3^{rd}$:$1/3^{rd}$ training:test data split, sampling equally across posttransplant function, we applied machine learning feature selection followed by protein-wise relaxed LASSO regression modeling, assessing the performance of the final set of protein models on the test data. Western blotting validated protein changes, and the biological relevance of the final set of protein models was externally validated by contextualization against a published dataset of human healthy and disease kidney transcriptomes.

Results. Our analysis revealed 144 proteins carrying outcome-predictive information, all of which showed donor-age modulated associations with posttransplant function, as opposed to age and protein/gene effects being independent terms. Observed associations with inflammatory, metabolic, protein processing and cell cycle pathways suggest biological targets for possible interventions pretransplant. Contextualization of our results against external spatial transcriptomic data suggest a sub-nephrotic spatial localization of the predictive signal.

Conclusions. Integrating kidney proteome information with clinical metadata enhances the resolution of donor kidney quality stratification, and the highlighted biological mechanisms open new research directions in developing predictive models and novel interventions during donor management or preservation to improve kidney transplant outcome.

SIGNIFICANCE STATEMENT

Currently, organ quality assessment pretransplant relies on key factors such as donor age or clinical information, these lack granularity in depicting graft susceptibility and capacity to function posttransplant. A high-resolution proteomic profiling of 185 pretransplant biopsies of kidneys with known posttransplant function and complete metadata was performed. Integration of donor kidney proteomes with 56 clinical metadata variables using regularized regression modelling resulted in enhancing the resolution of donor kidney quality stratification. Immuno-metabolic and catabolic processes contributed to donor kidney susceptibility and worse transplant outcomes in an age modulated pattern, validated by western blotting. Comparison of kidney proteomes with a recent transcriptomics dataset of healthy and diseased kidneys provide an additional special single cell resolution to the findings of this study.

INTRODUCTION

Kidney transplantation is the optimal treatment for end-stage kidney disease. Compared to dialysis, transplantation increases life-expectancy, improves quality of life and is cost-effective. Limited availability of suitable donor kidneys impedes treatment of chronic kidney disease, and often prolongs dialysis, increasing morbidity and mortality. Deceased donor organ shortages, living donation decline in some countries and emerging ageing populations drive increased utilization of older deceased donor kidneys, now comprising more than half of offered organs[1,2].

Ageing associates with time-dependent decline of organ function, evidenced in kidneys by histologic lesions, such as tubular atrophy, interstitial fibrosis, glomerulosclerosis, and arteriosclerosis. Older kidneys demonstrate fewer functioning glomeruli, less renal mass, podocyte dysfunction, and impaired cellular repair[3]. Glomerular diseases are more common and associated with worse outcomes in older patients[4]. Age accelerates the transition from Acute Kidney Injury (AKI) to chronic injury[5] and is an independent risk factor of graft dysfunction and loss for deceased donor kidneys[6]; furthermore, older donors are more likely to suffer from additional risk factors such as diabetes, hypertension or cardiovascular disease.

Donor age is incorporated in clinical scoring algorithms to inform kidney allocation decisions[7,8], but is insufficient to consistently predict transplant outcomes. Current front-line models incorporating further clinical factors such as terminal serum creatinine, history of hypertension and diabetes[8,9] show consistent performance across demographics but lack granular predictive accuracy[10].

Molecular analyses of biopsies plausibly offer higher resolution assessment of organ state; but require ‘big picture’ understanding of mechanisms associated specifically with poor

outcome, rather than immediate (but potentially recoverable) acute injury. Deceased donors are frequently assessed as having sustained damage (i.e. AKI) based on serum creatinine levels[11], however this metric poorly associates with longer term outcomes[11–14].

Mass spectrometry (MS) proteomic studies can provide such a 'big picture', but have heretofore lacked cohort capacity to represent demographic diversity[15]. Advances in high-throughput techniques[16] now allow sensitivity and depth without sacrificing throughput capacity. Developments in machine learning and nonlinear regression analyses furthermore offer tools to extract maximal knowledge from limited size experimental cohorts, with applications in disease staging, disease recurrence prediction, treatment response monitoring, and biomarker identification[17,18].

Integration of deep proteomic profiles with heterogenous clinical and demographic factors using modern statistical tools can empower the next steps toward precision medicine[19]. Here, we benefit from the granularity provided by our MS-based proteomic profiling to report age- and immunometabolism-related proteomic signatures in pre-implantation kidney biopsies associated with transplant outcomes.

METHODS

Study Design

Deceased donor pre-transplantation kidney biopsies (n=186; 1 sample excluded during data processing) were obtained from the Quality in Organ Donor (QUOD) biobank, a national multi-center UK wide bioresource of deceased donor clinical samples acquired during donor management and organ procurement. Biopsies were obtained from Donation after Brain Death

(DBD) donors and Donation after Circulatory Death (DCD) donors at the back table immediately after kidney procurement.

Selection of biopsies was based on paired 12-month post-transplant outcomes. To minimize the impact of recipient factors, we only included kidneys for which the contralateral kidney was transplanted with similar outcome. Kidneys were selected to cover the outcome continuum i.e. the range of estimated Glomerular Filtration Rate (eGFR) in the recipient at 12 months posttransplant (henceforth, 'eGFR12'), from primary non-function to eGFR>80 ml/min/1.73 m^2, excluding pediatric donors. Samples were linked to corresponding donor and recipient demographic and clinical metadata, provided by NHS Blood and Transplant National Registry.

Study Approval and Ethics statement

Informed consent from donor families was obtained prior to sample procurement. Collection of QUOD samples and research ethics approval was provided by QUOD (NW/18/0187).

Protein Extraction from Renal Tissue Specimens

Deceased donor biopsies were procured, handled and stored according to consistent, predefined collection protocols designed to minimize pre-analytical variability. Donor kidney biopsies were collected ex situ immediately after flush-out and procurement of the kidney in the donor hospital on the back-table. Biopsies were obtained from the upper pole of the donor kidney cortex during back table preparation, using a 23mm needle biopsy gun. The obtained biopsies were divided in two, with one half stored in RNAlater (Thermo Scientific, Illinois, USA), then liquid nitrogen and the other half stored in formalin.

RNAlater biopsy samples were homogenized in RIPA buffer (89900, Thermo Scientific, Illinois, USA) with protease and phosphatase inhibitor cocktail (1861280, Thermo Scientific, Illinois, USA) using a bead beater (Biorad, Hertfordshire, UK) at 6500rpm for three cycles of 40 seconds with intermediate cooling on wet ice between cycles. Biopsy protein concentration was determined using a Pierce Bicinchoninic Acid protein assay kit (23227 Thermo Scientific, Illinois, USA).

In-Solution Trypsin Digestion

50 µg of protein homogenates were prepared. Disulfide bonds were reduced by adding 200 mM of DTT (Sigma) to a final concentration of 5 mM for 60 mins at room temperature. Free cysteine residues were alkylated by adding 200 mM of iodoacetamide (Sigma) to a final concentration of 20 mM and incubated for 60 mins at RT in the dark.

The samples were topped up to 200 µl with 6 M urea, 100 mM TrisHCl pH 8.5. Methanol/chloroform protein precipitation was used to remove detergents before tryptic digestion. In brief, 600 µl of Methanol and 150 µl of Chloroform were added and mixed. Then 450 µl of MilliQ-H2O was added and then centrifuged for 1min at 12,000 g. The upper aqueous layer was carefully removed without disturbing formed protein pellets between layers and 450 µl of Methanol was added and then centrifuged at 12,000 g for 5 min. The supernatant was removed and the protein pellets resuspended in 50 µl of 6 M Urea, 100 mM TrisHCl, pH 8.5. Urea concentration was reduced to 1 M by adding 250 µl of MillQ-H2O. Samples were digested at 37 °C overnight with Trypsin added at a 1:50 ratio (trypsin:protein). Tryptic peptides were acidified and purified using Sep-Pak C18 cartridges (WAT020515, Waters, Wilmslow, UK) and dried by Speed Vac centrifugation. Pellets were resuspended in 80 µl of resuspension buffer A (98 % MilliQ-H2O, 2 % acetonitrile 0.1 % formic acid) for LC-MS/MS analysis.

Mass Spectrometry Analysis

Generation of Fractionated Pool for Spectral Library Reference

A highly fractionated spectral library was generated as a standard reference for the subsequent analysis of individual samples. To create this spectral library, a pool sample was prepared by combining 2 µl of each tryptic digest sample prepared above. Fractionation of the pooled sample was performed using offline high-pH reverse-phase HPLC on an XBridge BEH C18 XP column (3 × 150 mm, 2.5 µm pore size, Waters no. 186006710) over a 100-minute gradient (Buffer A: water, pH10 with ammonium hydroxide. Buffer B: 90 % acetonitrile, 10 % water, pH10 with ammonium hydroxide) with fractions collected every 2 minutes. The fractions of the pool sample for the spectral library were analyzed by nanoLC-MS/MS using a Dionex Ultimate 3000 using a 75 µm x 500 mm (2 µm particle size) C18 EASY-Spray column at 250 nL/min (Thermo Scientific), coupled to an Orbitrap Fusion Lumos mass spectrometer. Peptides were separated using a 60-minute linear gradient from 2-35 % buffer B (Buffer A: 5 % DMSO, 0.1 % formic acid in water. Buffer B: 5 % DMSO, 0.1 % formic acid in acetonitrile). The samples were analyzed on the mass spectrometer in Data-Dependent Acquisition mode. MS1 scans were acquired in the Orbitrap with an m/z range of 400 – 1500 m/z at a resolution of 120,000 and an AGC target of 4×10^5. Precursors between charge states 2+ and 7+ were selected for HCD fragmentation using the Advanced Precursor Determination option with an intensity threshold of 2.5×10^4. Selected precursors were isolated using the quadrupole with a 1.6 m/z isolation window and fragmented using HCD with a normalized collision energy of 30%. MS2 spectra were acquired in the Orbitrap using a resolution of 30,000, a maximum injection time of 54 ms and an AGC target of 5×10^4.

LC-MS/MS Analysis of Individual Biological Samples

The individual samples were analyzed on the same nanoLC-MS/MS system as above. A 45-minute linear gradient was used from 2-35 % buffer B with the same buffer composition as above. In contrast to the pool samples, the individual samples were analyzed using the SWATH DIA method [16]. The sample analysis order was randomized, and analyses of aliquots of the pooled sample used for library generation were scheduled every 20 runs throughout the sequence as a quality control. MS1 scans were acquired in the Orbitrap with an m/z range of 350 – 1650 m/z at a resolution of 120,000, an AGC target of 4 x 105 and a 3 second cycle time. MS2 scans were then acquired in stepped isolation windows with a 1 Th overlap between each window; first from 350-380 m/z up to 930-960 m/z in increments of 30 Th (i.e. 21 scans with midpoints of 365, 394 … 916, 945), followed by a 100 Th window scan of 959-1059 m/z and a 592 Th scan of 1058-1650 m/z.

Fragmentation of these windows was performed using a normalized collision energy of 25 % with a stepped collision energy of 10 %. MS2 spectra were acquired in the Orbitrap using a resolution of 30,000, a maximum injection time of 54 ms, an AGC target of 5 x 104 and a scan range of 360-1650 m/z.

Western Blot Validation

Samples were compared as 5 Upper Tertile (UT) versus 5 Lower Tertile (LT)within a single age category (younger; total n=20, or older; total n=20) on each gel. Kidney homogenates at 1µg/µL of protein were denatured at 90□C in Laemmli buffer and separated using 4-12% pre-cast Bis-Tris gels (Thermo Fisher Scientific, Massachusetts, USA) in the case of VTN and APOE western blots and 16% pre-cast Tricine gels (Thermo Fisher Scientific, Massachusetts, USA) in the case of PREB and CST3 western blots, in both cases using MOPS running buffer and followed by transfer onto a PVDF membrane (Thermo Fisher Scientific, Massachusetts,

USA). Membranes were then blocked in Intercept (TBS) Blocking Buffer (LiCOR P/N 927-60001) and incubated with primary antibodies overnight at 4 □C. Antibodies used were rabbit polyclonal anti-PREB (Thermo Fisher Scientific PA5-53125), mouse polyclonal anti-Vitronectin (R&D, MAB2349), rabbit monoclonal anti-APOE (16H22L18) (Thermo Fisher Scientific, 701241), rabbit monoclonal anti-CST3 (D6U3E) (Cell Signaling Technology, 24840) and mouse monoclonal anti-β-actin (Sigma, A5316) for protein normalization. The membranes were then incubated in species appropriate secondary antibodies (RDye® 800CW Goat anti-Mouse IgG Secondary Antibody and IRDye® 680RD Goat Anti-Rabbit IgG Secondary Antibody, LiCOR, USA). Finally, blots were imaged using the LI-COR Odyssey system (LiCOR, Nebraska, USA). Analysis and quantification were performed using LiCOR Image Studio (Version 2.2). Protein expression was normalized against β-actin and the fold change was calculated relative to the per-gel mean value of the Upper Tertile group. For each protein, fold changes relative to UT were combined across all gels within each age category, log2 transformed, and the difference between UT and LT calculated by t-testing without assumption of equal variance.

Statistical Analyses

Proteomic Data Processing

Both the DDA fractionated pools and all SWATH samples and pool data were analyzed simultaneously using DIA-NN v1.7.12 [20]. MS/MS spectra from the DDA pools were searched against UniProt Reference *Homo sapiens* database (retrieved 15/10/2020) with default settings, including 1 missed cleavage, oxidation of methionine as a variable modification and carbamidomethylation of cysteine as a fixed modification, to generate a spectral library. This

was then cross referenced against the SWATH data to quantify peptides, and thus proteins, within each SWATH sample and pool run. Precursor FDR was set to 1%.

Subsequent analysis of the DIA-NN output and integration with the clinical data was performed in R v4.0.2. One sample had extremely low average intensity and more than 15% missing values, so was eliminated from the analysis. Across the remaining 185 samples and pools, proteins with more than 50% missing values were eliminated. Intensity values were transformed by VSN (R package 'vsn' [21]), and the remaining missing values were imputed by a k-nearest neighbor approach (R package 'impute' [22]).

Clinical Variable Preprocessing

Clinical variables were subdivided into Donation after Brain Death (DBD)-specific variables, Donation after Cardiac Death (DCD)-specific variables and jointly applicable variables (see annotation, Supplementary Table 1). DBD- and DCD-specific variables were considered for the purposes of assessing correlation with outcome but were not considered for statistical analyses applied to the full dataset.

For significance testing of outcome differences between donor and recipient characteristics, and for all modelling, eGFR values for both donor measurements and recipient measurements at 12-month post-transplantation were stratified into tertiles - Lower Tertile (UT; eGFR < 40), Intermediate Tertile (IT; $40 \leq$ eGFR < 60) and Upper Tertile (UT; eGFR ≥ 60) based on their distribution. Missing values in the continuous and tertile-stratified forms of the variables were imputed for each sample by finding the 'set of neighbors' by 3-month eGFR, i.e. the 10 samples with the closest recipient eGFR at 3 months posttransplant, then taking the mean eGFR12 (ignoring any missing values) within that set of neighbors.

We curated the non-DBD/DCD specific clinical variables to remove those inappropriate for modelling (single-instance categories, variables which duplicated another variable in different units); the final list is given in Supplementary Table 2. HLA mismatches were modelled as 'Match Grade' with levels None; no mismatches, Favorable; no DR and one or fewer B mismatches, and Non-Favorable; at least one DR or two B mismatches (Supplementary Figure S2 and Supplementary Table ST1).

For curated clinical variables, missing values were imputed for each sample in a similar manner. A set of neighbors was built by finding the 10 samples with the smallest Gower's distance across all variables (multiple data types). We then took a relevant summary statistic of the non-missing values within the set of neighbors for each imputed value. For numeric values, the mean was taken. For categorical values, the most frequent category across the whole dataset was taken, breaking ties by iteratively shrinking the set of neighbors by removing the most distant from the sample to be imputed, until there was a single most frequent category.

Outcome Subgroup Comparison

Differences between outcome subgroups within DBD and DCD donor types (separately) were tested using Fisher's exact test for categorical variables and t-tests for numeric variables as appropriate.

Clinical variable association was calculated depending on the type of each variable in pairwise comparisons. Numeric-numeric comparisons were by Pearson's r. Numeric-categorical comparisons were by the square root of the proportion of variance explained (eta) from an ANOVA model where the numeric variable was taken as the response. Categorical-categorical comparisons were by Cramér's V. Hierarchical clustering was performed using the single-linkage method to avoid composition of comparison types.

The proteomic and clinical data were matched in R by sample identifier. Based on an initial scree plot of the variance distribution, unsupervised clustering of the proteomic data was performed by k-means clustering with k=4. The number of initial random centroids and the maximum number of iterations were both set to 10.

Training and Test Data Split

We split our data into a training and test sets, sampling equally across stratified eGFR. Of the 185 samples, 2/3 were used for training ('training set', 118 kidneys), and 1/3 were used for testing ('test set', 61 kidneys). Six paired kidneys (3 pairs) were reserved from both sets and used to assess MS and model performance ('QC set', 6 kidneys).

Machine Learning Feature Selection

Using sample assigned to the training dataset, we modelled the combined dataset of all protein abundance data plus the curated donor clinical variables (Supplementary Table S2) against ranked 12 month posttransplant eGFR, using Prediction Rule Ensemble (PRE) modelling (R package 'pre'[23]). We used the 'gpe' function allowing linear fits, decision tree fits and multivariate adaptive regression spline fits (via R package 'earth' [24]) to be considered for each ensemble. Decision tree learning was set to be 'random forest'-like, with 500 initial trees generated and boosting disabled to allow parallel processing. Other settings (including tree pruning and the parameters for linear and spline fits) were left as default; tree depth was therefore limited to the default 3 decision levels. Ensemble modelling was performed in an iterative manner. At each stage, modelling was performed on the set of predictors that excluded proteins listed in the final ensemble of all previous models. Clinical variables were never excluded. Modelling was repeated for 2000 iterations and all proteins appearing in any rule

ensemble, or with high correlation (Pearson's r>0.65) to any of these candidates, were selected for further analysis.

Regression Modelling

Based on the outcome of feature selection, we used regularized regression (relaxed LASSO, package 'glmnet', using the cv.glmnet function with 20-fold cross validation, selecting as the final model the model that maximized the shrinkage parameter lambda such that it was within 1 standard error of the lambda value that had the smallest cross-validation error, i.e. the 'lambda.1se' model) to regress each protein, donor age and protein:age terms against linearized outcome, defined as the proportion of eGFR12 values in the NHS Blood and Transplant National Registry between 2016 and 2021 inclusive (6 years) that were less than the observed eGFR12 (i.e. a normalization to population distribution quantile). An independent age-only model was also fit against the training dataset using the same parameters. For each protein model and the age-only model we calculated the prediction root-mean-square error (RMSE). Proteins with a higher RMSE than the independent donor age model, or whose model did not retain either the protein or protein:age term were discarded.

Functional Network Analysis

The final list of proteins resulting from regression modelling was queried using the Enrichr platform (R package 'enrichR'[25]) against the Reactome 2022 database. Annotation term assignments were filtered at 5% FDR. From the set of candidates with at least one assigned term across all three databases, a connection graph was generated (R package 'igraph'[26]) with nodes representing proteins and edges representing shared annotation terms. Nodes (proteins) were clustered using the walktrap community detection algorithm[27] as implemented in igraph. Within-community enrichment for annotation terms was calculated by Fisher's exact test.

Age-Protein-Outcome Clustering

For each protein, eGFR12 was predicted using the corresponding relaxed LASSO model for donor ages 20,21,22…80 and protein quantiles 0,0.01,0.02…1, resulting in a 61x101 matrix. Matrix-matrix distances were computed using the Frobenius distance (R package 'StatPerMeCo'[28]), and proteins were clustered according to these pairwise distances by hierarchical clustering.

Spatial Correlation Analysis

Processed, normalized AKI and CKD spatial scRNA-seq expression data generated by Lake *et al.*[29] were obtained from CELLxGENE (https://cellxgene.cziscience.com/collections/bcb61471- 2a44-4d00-a0af-ff085512674c). Proteins identified by feature selection and LASSO regression filtering were matched to the expression dataset by the 'Genes' column in the DIA-NN output. AKI:CKD correlation in matched versus unmatched genes in each characterized spatial location was compared using the approach described by Fisher[30] (R package 'cocor'[31]).

RESULTS

Selected Samples were Demographically Balanced Across Outcome Strata

Samples were selected to provide a balanced representation of the UK donor population (Table 1) and reproduced generally observed trends in terms of the correlation between eGFR12 and clinical variables; we found the strongest associations were donor age (Pearson's r=-0.52), and recipient age (r=-0.28) (Supplementary Figure S1).

For an interpretable analysis of key clinical factors, we considered our samples by eGFR12 stratum Lower Tertile (LT; eGFR12 < 40), Intermediate Tertile (IT; 40≤eGFR12<60), and Upper Tertile (UT; eGFR12≥60) all units ml/min/1.73 m^2 (Figure 1). We investigated associations between clinical variables and stratified eGFR12 subgroups within each donor type, and between donor types within stratified eGFR12 subgroups (Supplementary Table ST1); the only variables with significant difference between outcome groups across donor types were the UK Kidney Donor Risk Index; UKKDRI[8] (ANOVA F-test; DBD: p=1.298e-6; DCD: p=3.946e-7), donor age (ANOVA F-test; DBD: p=1.253e-9; DCD: p=1.196e-7), histories of hypertension (ANOVA F-test; DBD: p=0.0020; DCD: p=0.1069). Histories of diabetes (ANOVA F-test; p=0.6188; DCD: p=0.2348) and terminal serum creatinine levels (ANOVA F-test; DBD: p=0.6972; DCD: p=0.6448) were similar across outcome subgroups although the latter was higher in DBD than in DCD in the UT group (t-test; p=0.0443).

Integration of Kidney Proteomes with Clinical Metadata by Rule Ensemble and Regression Modelling Identifies Outcome-Associated Proteins

Proteomic analysis quantified 2984 protein groups with 50% or less missing values (out of 7790 identified protein groups in total) over 185 samples and 20 interspersed sample pools (Supplementary Figure S2A). Analysis of sample pools showed minimal sample acquisition-related variance (squared mean pairwise Z-corrected Pearson's *r*=0.94). The 3 pairs of kidneys showed high correlation of protein intensity values between donor pairs (Pearson's *r*=0.71, 0.92 and 0.91; Supplementary Figure S2B).

We initially explored the proteomic data using Principal Component Analysis (PCA) to find underlying linear trends. Sample variance concentrated in the first two principal components (PC1: 20.01%; PC2: 13.38%; Figure S3). K-means clustering identified 4 distinct clusters

(Figure S3; Figure S4A) which associated with donor type, with a preponderance of DBD samples towards Cluster 2 and a preponderance of DCD samples towards Cluster 4 (Figure S4B, upper left panel; p=0.0235), but did not associate strongly with recipient eGFR (p=0.4134), donor eGFR (p=0.1684), or donor age (p=0.7907) (Figure S4B, upper middle, upper right and lower left panels). There was a weakly significant association between cluster membership and donor BMI (p=0.0350) and with donor serum creatinine (p=0.0326) (Figure S4B, lower middle and lower right panels).

To assess individual protein relationships with outcome, we adopted a descriptive modelling approach, using a subset of our data ('training set'; 2/3 of data) to find protein models which predicted eGFR12 better than donor clinical data alone, then assessing model performance against unseen (i.e. held out) test data ('test set', 1/3 of data). Six of the kidneys analyzed (3 pairs) were pairs from the same donor; these were reserved from both training and test data for quality control ('QC set', 6 kidneys). To create our train/test split, we randomly selected equal numbers of samples for the training set within each of the eGFR12 strata described above, to sample equally across outcome range.

To identify possible outcome-associated proteins, relevant clinical variables and potential protein-clinical variable interactions, we used iterative Prediction Rule Ensembles[23] (PRE) learning on our training set to select features among the set of quantified proteins and donor type-independent donor clinical variables. Briefly, PRE identifies a minimal ensemble of explanatory rule (functions of variables) for a given response (here, ranked eGFR12) allowing for nonlinear associations and variable interactions. To build a catalog (rather than minimal set) of explanatory proteins, we repeated our analysis 2000 times, removing proteins identified in the rule ensemble at each iteration from the dataset for future iterations, retaining clinical variables.

This process generated 195 candidate proteins; we further supplemented this list with proteins that had high correlation (Pearson's r>0.65) with any of those candidates; bringing the final list up to 255 candidates.

The only donor clinical variable term to feature consistently in rule ensembles was donor age, appearing in all 2000 ensembles generated. We individually tested each protein candidate for association with outcome, including protein, donor age, and age:protein interaction terms using LASSO regression[32] to aim for the simplest explanatory models (i.e. that include only the minimum necessary terms). To ensure models would generalize beyond our data, for the final modelling we linearized the eGFR12 measurement against UK NHS Blood and Transplant National Registry data. We discarded candidates whose model discarded both the protein and age:protein terms, or had a higher root-mean-square error (RMSE) of prediction than a model built with donor age alone.

After filtering we had identified 144 proteins which associated with outcome (Supplementary Table 2). The mean RMSE of our protein models was 25.76 ml/min/1.73m^2 in our training data, and fell slightly to 22.25 ml/min/1.73m^2 in our test data, indicating the models were not over-fit (Supplementary Figure S5).

Functional Analysis of Outcome-Associated Proteins Reveals Immuno-Metabolic Pathway Clusters

We performed a network analysis of shared Reactome pathways (Figure 2A). Walktrap clustering revealed 4 major clusters of shared-pathway proteins (Table 2); Immune Regulation & Complement Activation, Metabolism, Protein Metabolism & Modification, and Cell Cycle. To validate our findings, we selected three representative proteins with available antibodies and known biological relevance (Vitronectin (VTN); fibrosis, Apolipoprotein E (APOE); CKD risk,

Cystatin C (CST3); nephron function) and confirmed that all three showed differences between low and high eGFR outcome sample subgroups by western blot (Figure 2B). Furthermore, all three proteins consistently predicted similar outcomes for each pair of kidneys within the triple-pair QC set, and correctly separated the two below-median outcome (eGFR12<50) pairs from the above-median outcome (eGFR12>50) pair (Figure S6).

Association of Proteins with Posttransplant Outcome is Modulated by Donor Age

For all 144 proteins, the minimal model retained an age:protein interaction term where the predictive effect of protein abundance was modulated by age, independent of the effect of age alone or protein abundance alone (Supplementary Table 2). To visualize these effects, we used each model to predict eGFR12 across increasing donor age and protein quantile. The interplay between protein quantile and age could be broadly grouped (by hierarchical clustering) into 3 clusters with protein to eGFR12 associations that showed different patterns across donor age (Figure 3), with about a third (31%) of candidates, including CST3, falling into a cluster with a profound effect of age on protein to eGFR12 association at high donor age.

Comparison to Spatial scRNA-Seq Data Reveals Localization of Outcome-Associated Signal

As an independent validation of our findings, we sought to contextualize them in the wider context of kidney damage. To do this, we compared the expression levels of our candidate protein set to a recent spatial scRNA-seq dataset comparing AKI and CKD[29]. This initial comparison revealed that all 144 of our candidates were matched to transcripts reported in this external dataset, and, consistent with our proteomic data. Two of our highlighted candidates associated with outcomes, APOE and CST3, were also highlighted as associated with fibrosis and inflammation damaged tubules in this dataset.

We then investigated how the expression levels of transcripts corresponding to our set of 144 proteins changed between AKI and CKD. We reasoned that protein and gene expression data that carries outcome-predictive information must reflect differences in organ injury. Therefore, between different injurious scenarios, we would expect gene expression that is predictive (i.e. discriminatory) to have lower correlation than genes whose expression change was linked to general inflammation and stress response. We compared the AKI:CKD expression correlation of our set of candidates versus the expression correlation of all other transcripts in the dataset. Since the dataset is spatially resolved, we were able to make this comparison across regions of the nephron. We observed that our candidate protein set had stronger discriminatory power (i.e. significantly lower correlation; Fisher test, p=4.04e-11) than background in distal convoluted tubule epithelial cells and in surrounding structures, but not in leukocytes or in globally aggregated data (Figure 4).

This result gave us confidence that the 144-candidate set we report represents signatures of specific organ injury, and suggests that proteomic signals in distal convoluted tubule may be particularly representative of the extent to which injury impacts future functionality.

DISCUSSION

This study presents the first large unbiased human kidney tissue proteomics dataset for deceased donor kidneys. We examined the relationship between posttransplant kidney function with pretransplant kidney proteomes by analyzing 185 deceased donor kidneys with complete donor and recipient associated metadata. Although our study was not aiming to report a single biomarker, our large cohort, our unique machine learning approach, and finally alignment of proteomic data with a large spatial single cell transcriptomics dataset on healthy and diseased kidney substantiates our key findings. We describe an integration of kidney proteome with

clinical metadata and show that modelling age modulation of proteomic signals provides enhanced resolution of donor kidney quality stratification and highlights biological mechanisms.

Our analysis reveals the importance of integrating across both subclinical and clinical data. Exploring our data using iterative PRE feature selection, a substantial number of proteins were revealed to be relevant, but only one clinical variable, donor age. Donor age is a key contributor in clinical decisions and is a strongly weighted term in extant kidney allocation scoring systems [8,33], but in the case of all reported candidate proteins, prediction models retained a protein:donor age interaction term. This second-order effect has not (to our knowledge) been explored in transplantation, and may be important to fully understanding molecular predictors.

A clinical variable notable by its omission from our association findings was donor type[34]. It is possible that outcome-predictive information 'carried' by donor type is also derivable from the proteome (proteomic data were able to partially distinguish samples based on type even when considering only variance across linear combinations of proteins; Figure S4). Without disputing donor type-specific mechanisms of kidney damage[35], our data are consistent with the idea that location and type of damage may be a greater contributor towards recovery potential[36] than mechanism of injury.

Kidney metabolism is altered as a result of biological stress occurring during donor management, in both DBDs and DCDs[37]. Within our final list of 144 proteins associated with outcome there is a common theme of implication in immune response to kidney injury (including both chronic injury, and acute injury) as a result of metabolic disruption, particularly responses associated with ischemia. We highlighted three proteins from our set of 144 outcome-associated candidates as a sanity check; all three are examples of known chronic damage indicators that we find here to have a donor organ pre-transplant predictive association.

Vitronectin (VTN) is a primary component of the extracellular matrix involved in cell adhesion, enhancing the activity of plasminogen activator inhibitor-1 and inhibition of the terminal complement pathway[38], and is a potential fibrotic biomarker[39].

Apolipoprotein E (APOE) stands out as having previously reported genetic allele age-related associations with disease and organ dysfunction including risk of Alzheimer's Disease[40] (with the strongest effect manifesting around age 65[41]), macular dysfunction, atherosclerosis and pulmonary scarring[42,43], and evidence for shared allele risk across diseases[44]. In kidneys, APOE plays an important role in lipid metabolism to regulate the growth and survival of mesangial cells and preserve organ function[45]; it is a marker for outcome in transplant recipients[46–48], and there is evidence for *APOE* genotype association with kidney dysfunction risk[49–51], possibly manifested by lipidomic differences between allelic profiles[52]. We have previously reported small (not statistically significant) increases in APOE due to ischemic reperfusion injuries[53] possibly explained by a role in senescence mediation[54]. There is existing evidence for similar allele dependent transplant outcome effects in another apolipoprotein (APOL1)[55], suggesting that both *APOE* genotype and the broader apolipoprotein allelic profile may play an important role in posttransplant graft function.

Cystatin C (CST3) is particularly noteworthy as, measured in serum, it is a known and effective general biomarker for kidney function and has predictive power for outcomes in transplant recipients[56–58]. Our evidence indicates a further association between CST3 levels in donor kidney tissue and outcome; moreover, that this effect is age dependent, starting around age 40. Serum CST3 is relatively independent of age in children and young adults[59], but may also show age association in later years[60].

A potential hurdle in contextualizing our findings in existing orthogonal transcriptomic data was that proteomes and transcriptomes are generally poorly correlated in terms of abundance changes[61]. In order to avoid this problem, we considered how the pattern of injury scenario-related differences changed between predictive and background signals within the same transcriptomic dataset[29]. The spatial component of this dataset further allowed us to show that injury-specific signals within our 144-protein set localized most strongly to the distal convoluted tubule (DCT) epithelium. Damage to DCT epithelial cells can be predictive of outcome[62]; the interplay of proximal and distal injury is complex[63], but previous work has suggested that DCT epithelial cells can play an important protective and damage repair role across the nephron, expressing survival and reparative factors in response to injury[64]. Indications that aging is associated with accumulation of senescent epithelial cells with a maladaptive stress response[29] suggest a mechanism whereby aging related senescent cell accumulation could reduce the ability of DCT epithelia cells to protect and promote recovery of injury sustained by the proximal tubules. This would be consistent with our findings (immuno-metabolic and ischemia response functional association, and spatially localized response) and the negative donor age correlation with transplant outcome, and might explain recent successes with senescence inhibitors in treating CKD[65], suggesting that routes to stimulate or enhance the DCT regenerative effect could be avenues for organ preservation.

Our list of outcome-associated candidates cannot be exhaustive. Practicalities of sample acquisition limited sampling of a wide range of outcomes outside the 30-60 donor age range, especially limited Upper Tertile outcome events in older donors. Organ allocation algorithms impose a close link between donor and recipient age in the sample cohort, so while we interpret these age-moderated effects in terms of organ resilience in older donors, it could also represent a

525 greater ability to repair a given level of damage in younger recipients. Further, we consider only
526 chronological donor age, rather than a more nuanced representation of the epigenomic biological
527 clock [66], which may to account for some variation observed with respect to both donors and
528 recipients.

529 It is immediately clear from our results that the strength of the donor age factor is
530 enormous relative to any other protein or clinical effect; this age effect is liable to dominate any
531 prediction weighting and reduce the accuracy of estimated protein contribution. A much larger
532 cohort could mitigate this issue, especially if paired with variant sequencing to understand
533 genetic diversity. Advances in high-throughput proteomics techniques continue to increase
534 feasible cohort sizes[67] but fundamental limitations on organ acquisition remain. Archiving at
535 scale of clinical samples in bioresources such as the QUOD biobank to parallel advancements in
536 big data analysis and interpretation platforms is therefore necessary for future development of
537 granular evidence-based decision making.

538 However, given the limitations of our dataset, our protein models generalized well to
539 samples unseen during model training (Figure S5), and showed promise for outcome-
540 classification prediction (Figure S6) suggesting that, with a larger training cohort to address the
541 caveats acknowledged above, a substantial component of early posttransplant outcome may be
542 predictable solely using subclinical measurements moderated by donor age. The biological
543 themes of the 144 proteins identified herein reinforce known immuno-metabolic mechanisms of
544 kidney injury but raise interesting possibilities for further work, especially with regard to donor
545 genetic background, and also suggest that the possibility of donor age-moderated weighting
546 should be considered as a matter of course in future work.

547

SUPPLEMENTARY MATERIALS

Supplementary Table ST1: Clinical variable p-values for association with donor type and outcome.

Supplementary Table ST2: Summary of results for all candidate proteins.

Note that coefficient values provided are for linearized eGFR12, i.e. they relate to eGFR12 quantile ranging from 0 to 1.

Supplementary Figure S1: Donor and recipient clinical and demographic data association with recipient 12-month eGFR rank.

Single-linkage hierarchical clustering of curated, imputed clinical variables by relative association strength (taking distance as 1-association). The outcome variable (ranked recipient eGFR at 12 months post-transplantation) is highlighted in red.

Supplementary Figure S2: Protein quantification quality.

A: Missingness comparison: Proteins are shown ranked by the number of missing values across all samples and the twenty standard pools, excluding one run which was removed due to low signal. 2984 proteins had missing values in 50% or less runs.

B: Paired Kidney Comparison: Protein abundance values from paired kidneys (left/right) from 3 individual donors were compared, as these are effectively biological replicates. x axes: value in left kidney. y axes: value in right kidney. Inset: Pearson's r correlation coefficient.

Supplementary Figure S3: Scree plot of variance represented by the first ten principle components in the proteomic data.

A reasonable number for the cluster parameter (k) supplied for k-means clustering (see Figure S4) lay between 3 and 5 based on the 'elbow' method'; we selected k=4.

Supplementary Figure S4: Unbiased analysis of pretransplant kidney proteomes and cluster associations.

A: Unbiased analysis of proteomic data by k-means clustering. Sample separation by Principal Component Analysis. Top Left: Samples were assigned to four clusters by k-means. Bottom & Right: There was a difference in the distribution of DBD and DCD donors across clusters, with the DBD donors being more heavily concentrated in Cluster 2 ('+' symbol; orange shading), and DCD in Cluster 4 ('x' symbol; pink shading)

B: There were no associations between proteome clusters and most donor and recipient factors, except for mildly significant differences in donor BMI and creatinine (selected comparisons shown; left-right, top-bottom: donor type, recipient 12-month posttransplant eGFR (outcome), donor eGFR, donor age, donor BMI, donor creatinine at retrieval).

Supplementary Figure S5: Performance of individual protein with age models on unseen data.

For each protein, the protein term plus age term and protein:age interaction term were modelled against linearized 12-month posttransplant eGFR (eGFR12) using LASSO. For proteins passing filtering, with eGFR root-mean-square error (RMSE) better than an age-only model, we compared the RMSE achieved on the model training data against the RMSE achieved on held-out test data. We observed that the models actually achieved slightly better performance on the test data, reassuring us that no model was over-fit to the training data (i.e. all models generalized well to unseen data).

Supplementary Figure S6: Performance of VTN, APOE and CST3 models on paired kidney data.

Six of the analyzed kidneys were paired (i.e. two came from each of three donors). These data were not used for training or testing but reserved for QC of the proteomics (Figure S2). Although our analysis was focused on identification of outcome-associated protein

signals rather than prediction of eGFR12 (due to cohort size limitations, we do not claim to have a maximally biologically representative training set), we nevertheless used these paired kidneys to assess the consistency of our modelling in predicting above/below median outcomes in the three proteins we highlighted as particularly interesting. In all three pair cases the outcomes in (different) recipients were similar within each pair, and for all three proteins the model consistently predicted the correct above/below median classification for all six kidneys.

DATA AND MATERIALS AVAILABILITY

The mass spectrometry proteomics data have been deposited to the ProteomeXchange Consortium via the PRIDE [68] partner repository with the dataset identifier PXD033428.

DISCLOSURE AND FUNDING

This study was supported by NHS Blood and Transplant funding awarded to MK & RJP. SF was supported by Kidney Research UK, grant reference KS_RP_002_20210111 awarded to MK. PDC was supported by a Chinese Academy of Medical Sciences 2018-I2M-2-002 awarded to BMK. Authors declare that they have no competing interests.

Author contributions:

Conceptualization: MK

Methodology: PDC, SF, RV, SD, RF, BMK, AS, ES, RJP, MK

Investigation: PDC, SF, RV, PJ, SD, IV, KT, AS

Visualization: PDC

Funding acquisition: BMK, RJP, MK

Project oversight: MK

Supervision: RF, AS, MK

Writing – original draft: PDC, ES, MK

Writing – review & editing: All authors

REFERENCES

1. Callaghan CJ, Mumford L, Pankhurst L, Baker RJ, Bradley JA, Watson CJE. Early Outcomes of the New UK Deceased Donor Kidney Fast-Track Offering Scheme. *Transplantation*. 2017;101(12):2888-2897. doi:10.1097/TP.0000000000001860

2. Summers DM, Johnson RJ, Hudson AJ, et al. Standardized deceased donor kidney donation rates in the UK reveal marked regional variation and highlight the potential for increasing kidney donation: a prospective cohort study†. *Br J Anaesth*. 2014;113(1):83-90. doi:10.1093/bja/aet473

3. Denic A, Glassock RJ, Rule AD. The Kidney in Normal Aging: A Comparison with Chronic Kidney Disease. *Clin J Am Soc Nephrol*. 2022;17(1):137-139. doi:10.2215/CJN.10580821

4. O'Hare AM, Choi AI, Bertenthal D, et al. Age affects outcomes in chronic kidney disease. *J Am Soc Nephrol*. 2007;18(10):2758-2765. doi:10.1681/ASN.2007040422

5. Ishani A, Xue JL, Himmelfarb J, et al. Acute Kidney Injury Increases Risk of ESRD among Elderly. *J Am Soc Nephrol*. 2009;20(1):223-228. doi:10.1681/ASN.2007080837

6. Summers DM, Johnson RJ, Hudson A, Collett D, Watson CJ, Bradley JA. Effect of donor age and cold storage time on outcome in recipients of kidneys donated after circulatory death in the UK: a cohort study. *Lancet*. 2013;381(9868):727-734. doi:10.1016/S0140-6736(12)61685-7

7. Rao PS, Schaubel DE, Guidinger MK, et al. A comprehensive risk quantification score for deceased donor kidneys: the kidney donor risk index. *Transplantation*. 2009;88(2):231-236. doi:10.1097/TP.0b013e3181ac620b

8. Watson CJE, Johnson RJ, Birch R, Collett D, Bradley JA. A Simplified Donor Risk Index for Predicting Outcome After Deceased Donor Kidney Transplantation. *Transplantation*. 2012;93(3):314-318. doi:10.1097/TP.0b013e31823f14d4

9. Neuberger J, Callaghan C. Organ utilization - the next hurdle in transplantation? *Transpl Int*. 2020;33(12):1597-1609. doi:10.1111/tri.13744

10. Clayton PA, Dansie K, Sypek MP, et al. External validation of the US and UK kidney donor risk indices for deceased donor kidney transplant survival in the Australian and New Zealand population. *Nephrol Dial Transplant*. 2019;34(12):2127-2131. doi:10.1093/NDT/GFZ090

11. Yu K, Husain SA, King K, Stevens JS, Parikh CR, Mohan S. Kidney nonprocurement in deceased donors with acute kidney injury. *Clin Transplant*. Published online August 4, 2022:e14788. doi:10.1111/ctr.14788

12. Hall IE, Akalin E, Bromberg JS, et al. Deceased-donor acute kidney injury is not associated with kidney allograft failure. *Kidney Int*. 2019;95(1):199-209. doi:10.1016/j.kint.2018.08.047

13. Liu C, Hall IE, Mansour S, Thiessen Philbrook HR, Jia Y, Parikh CR. Association of Deceased Donor Acute Kidney Injury With Recipient Graft Survival. *JAMA Network Open*. 2020;3(1):e1918634. doi:10.1001/jamanetworkopen.2019.18634

14. Mansour SG, Khoury N, Kodali R, et al. Clinically adjudicated deceased donor acute kidney injury and graft outcomes. *PLoS One*. 2022;17(3):e0264329. doi:10.1371/journal.pone.0264329

15. von Moos S, Akalin E, Mas V, Mueller TF. Assessment of Organ Quality in Kidney Transplantation by Molecular Analysis and Why It May Not Have Been Achieved, Yet. *Front Immunol*. 2020;11:833. doi:10.3389/fimmu.2020.00833

16. Gillet LC, Navarro P, Tate S, et al. Targeted data extraction of the MS/MS spectra generated by data-independent acquisition: a new concept for consistent and accurate proteome analysis. *Mol Cell Proteomics*. 2012;11(6):O111.016717. doi:10.1074/mcp.O111.016717

17. Geyer PE, Holdt LM, Teupser D, Mann M. Revisiting biomarker discovery by plasma proteomics. *Mol Syst Biol*. 2017;13(9):942. doi:10.15252/msb.20156297

18. Connor KL, O'Sullivan ED, Marson LP, Wigmore SJ, Harrison EM. The Future Role of Machine Learning in Clinical Transplantation. *Transplantation*. 2021;105(4):723-735. doi:10.1097/TP.0000000000003424

19. Raynaud M, Aubert O, Divard G, et al. Dynamic prediction of renal survival among deeply phenotyped kidney transplant recipients using artificial intelligence: an observational, international, multicohort study. *The Lancet Digital Health*. 2021;3(12):e795-e805. doi:10.1016/S2589-7500(21)00209-0

20. Demichev V, Messner CB, Vernardis SI, Lilley KS, Ralser M. DIA-NN: neural networks and interference correction enable deep proteome coverage in high throughput. *Nat Methods*. 2020;17(1):41-44. doi:10.1038/s41592-019-0638-x

21. Huber W, von Heydebreck A, Sultmann H, Poustka A, Vingron M. Variance stabilization applied to microarray data calibration and to the quantification of differential expression. *Bioinformatics*. 2002;18(Suppl 1):S96-S104. doi:10.1093/bioinformatics/18.suppl_1.S96

22. Hastie T, Tibshirani R, Narasimhan B, Chu G. *Impute: Imputation for Microarray Data*.; 2021. http://www.bioconductor.org/packages/release/bioc/html/impute.html

686 23. Fokkema M. Fitting prediction rule ensembles with R package pre. *J Stat Softw*.
687 2020;92(1):1-30. doi:10.18637/jss.v092.i12

688 24. Milborrow. Derived from mda:mars by T. Hastie and R. Tibshirani. S. *Earth: Multivariate*
689 *Adaptive Regression Splines*.; 2011. http://CRAN.R-project.org/package=earth

690 25. Jawaid W. *EnrichR: Provides an R Interface to "Enrichr."*; 2021. https://cran.r-
691 project.org/package=enrichR

692 26. Csárdi G, Nepusz T. The igraph software package for complex network research.
693 *InterJournal*. 2006;Complex Systems:1695.

694 27. Pons P, Latapy M. *Computing Communities in Large Networks Using Random Walks*.
695 (Yolum P, Güngör T, Gürgen F, Özturan C, eds.). Springer; 2005. doi:10.1007/11569596_31

696 28. Trucios C. *StatPerMeCo: Statistical Performance Measures to Evaluate Covariance Matrix*
697 *Estimates*.; 2017. https://CRAN.R-project.org/package=StatPerMeCo

698 29. Lake BB, Menon R, Winfree S, et al. An atlas of healthy and injured cell states and niches in
699 the human kidney. *Nature*. 2023;619(7970):585-594. doi:10.1038/s41586-023-05769-3

700 30. Fisher RA. *Statistical Methods for Research Workers*. Oliver and Boyd; 1925.
701 https://openlibrary.org/books/OL17638383M.opds

702 31. Diedenhofen B, Musch J. cocor: A Comprehensive Solution for the Statistical Comparison
703 of Correlations. *PLoS ONE*. 2015;10(4):e0121945. doi:10.1371/journal.pone.0121945

704 32. Friedman JH, Hastie T, Tibshirani R. Regularization Paths for Generalized Linear Models
705 via Coordinate Descent. *J Stat Softw*. 2010;33:1-22. doi:10.18637/jss.v033.i01

706 33. Li B, Cairns JA, Robb ML, et al. Predicting patient survival after deceased donor kidney
707 transplantation using flexible parametric modelling. *BMC Nephrol*. 2016;17(1):51.
708 doi:10.1186/s12882-016-0264-0

709 34. Gill J, Rose C, Lesage J, Joffres Y, Gill J, O'Connor K. Use and Outcomes of Kidneys from
710 Donation after Circulatory Death Donors in the United States. *J Am Soc Nephrol*.
711 2017;28(12):3647-3657. doi:10.1681/asn.2017030238

712 35. Vaughan RH, Kresse JC, Farmer LK, et al. Cytoskeletal protein degradation in brain death
713 donor kidneys associates with adverse post-transplant outcomes. *Am J Transplant*. Published
714 online December 8, 2021. doi:10.1111/ajt.16912

715 36. Kosmoliaptsis V, Salji M, Bardsley V, et al. Baseline donor chronic renal injury confers the
716 same transplant survival disadvantage for DCD and DBD kidneys. *Am J Transplant*.
717 2015;15(3):754-763. doi:10.1111/ajt.13009

718 37. Damman J, Bloks VW, Daha MR, et al. Hypoxia and Complement-and-Coagulation
719 Pathways in the Deceased Organ Donor as the Major Target for Intervention to Improve
720 Renal Allograft Outcome. *Transplantation*. 2015;99(6):1293-1300.
721 doi:10.1097/TP.0000000000000500

38. De Lorenzi V, Sarra Ferraris GM, Madsen JB, Lupia M, Andreasen PA, Sidenius N. Urokinase links plasminogen activation and cell adhesion by cleavage of the RGD motif in vitronectin. *EMBO Rep*. 2016;17(7):982-998. doi:10.15252/embr.201541681

39. Carreras-Planella L, Cucchiari D, Cañas L, et al. Urinary vitronectin identifies patients with high levels of fibrosis in kidney grafts. *J Nephrol*. 2021;34(3):861-874. doi:10.1007/s40620-020-00886-y

40. Liu CC, Kanekiyo T, Xu H, Bu G. Apolipoprotein E and Alzheimer disease: risk, mechanisms, and therapy. *Nat Rev Neurol*. 2013;9(2):106-118. doi:10.1038/nrneurol.2012.263

41. Saddiki H, Fayosse A, Cognat E, et al. Age and the association between apolipoprotein E genotype and Alzheimer disease: A cerebrospinal fluid biomarker-based case-control study. *PLoS Med*. 2020;17(8):e1003289. doi:10.1371/journal.pmed.1003289

42. Mahley RW, Rall SC. Apolipoprotein E: far more than a lipid transport protein. *Annu Rev Genomics Hum Genet*. 2000;1:507-537. doi:10.1146/annurev.genom.1.1.507

43. Yao X, Gordon EM, Figueroa DM, Barochia AV, Levine SJ. Emerging Roles of Apolipoprotein E and Apolipoprotein A-I in the Pathogenesis and Treatment of Lung Disease. *Am J Respir Cell Mol Biol*. 2016;55(2):159-169. doi:10.1165/rcmb.2016-0060TR

44. Miwa K, Tanaka M, Okazaki S, et al. Chronic kidney disease is associated with dementia independent of cerebral small-vessel disease. *Neurology*. 2014;82(12):1051-1057. doi:10.1212/WNL.0000000000000251

45. Chen G, Paka L, Kako Y, Singhal P, Duan W, Pillarisetti S. A Protective Role for Kidney Apolipoprotein E: REGULATION OF MESANGIAL CELL PROLIFERATION AND MATRIX EXPANSION. *J Biol Chem*. 2001;276(52):49142-49147. doi:10.1074/JBC.M104879200

46. Kahraman S, Kiykim AA, Altun B, et al. Apolipoprotein E gene polymorphism in renal transplant recipients: effects on lipid metabolism, atherosclerosis and allograft function. *Clin Transplant*. 2004;18(3):288-294. doi:10.1111/j.1399-0012.2004.00162.x

47. Hernández D, Salido E, Linares J, et al. Role of apolipoprotein E epsilon 4 allele on chronic allograft nephropathy after renal transplantation. *Transplant Proc*. 2004;36(10):2982-2984. doi:10.1016/j.transproceed.2004.10.038

48. Cofán F, Cofan M, Rosich E, et al. Effect of apolipoprotein E polymorphism on renal transplantation. *Transplant Proc*. 2007;39(7):2217-2218. doi:10.1016/j.transproceed.2007.06.011

49. Czaplińska M, Ćwiklińska A, Sakowicz-Burkiewicz M, et al. Apolipoprotein e gene polymorphism and renal function are associated with apolipoprotein e concentration in patients with chronic kidney disease. *Lipids Health Dis*. 2019;18(1):1-9. doi:10.1186/s12944-019-1003-x

50. Hsu CC, Kao WHL, Coresh J, et al. Apolipoprotein E and progression of chronic kidney disease. *J Am Med Assoc*. 2005;293(23):2892-2899. doi:10.1001/jama.293.23.2892

51. Saito T, Ishigaki Y, Oikawa S, Yamamoto TT. Etiological significance of apolipoprotein E mutations in lipoprotein glomerulopathy. *Trends Cardiovasc Med*. 2002;12(2):67-70. doi:10.1016/S1050-1738(01)00148-7

52. Sienski G, Narayan P, Bonner JM, et al. APOE4 disrupts intracellular lipid homeostasis in human iPSC-derived glia. *Sci Transl Med*. 2021;13(583):eaaz4564. doi:10.1126/scitranslmed.aaz4564

53. Huang H, van Dullemen LFA, Akhtar MZ, et al. Proteo-metabolomics reveals compensation between ischemic and non-injured contralateral kidneys after reperfusion. *Sci Rep*. 2018;8(1):8539. doi:10.1038/s41598-018-26804-8

54. Zhao H, Ji Q, Wu Z, et al. Destabilizing heterochromatin by APOE mediates senescence. *Nature Aging*. 2022;2(4):303-316. doi:10.1038/s43587-022-00186-z

55. Julian BA, Gaston RS, Brown WM, et al. Effect of Replacing Race with Apolipoprotein L1 Genotype in Calculation of Kidney Donor Risk Index. *Am J Transplant*. 2017;17(6):1540. doi:10.1111/AJT.14113

56. Coll E, Botey A, Alvarez L, et al. Serum cystatin C as a new marker for noninvasive estimation of glomerular filtration rate and as a marker for early renal impairment. *Am J Kidney Dis*. 2000;36(1):29-34. doi:10.1053/ajkd.2000.8237

57. Christensson A, Ekberg J, Grubb A, Ekberg H, Lindström V, Lilja H. Serum cystatin C is a more sensitive and more accurate marker of glomerular filtration rate than enzymatic measurements of creatinine in renal transplantation. *Nephron Physiol*. 2003;94(2):19-27. doi:10.1159/000071287

58. Rodrigo E, Ruiz JC, Fernández-Fresnedo G, et al. Cystatin C and albuminuria as predictors of long-term allograft outcomes in kidney transplant recipients. *Clin Transplant*. 2013;27(2):E177-83. doi:10.1111/ctr.12082

59. Bökenkamp A, Domanetzki M, Zinck R, Schumann G, Byrd D, Brodehl J. Cystatin C--a new marker of glomerular filtration rate in children independent of age and height. *Pediatrics*. 1998;101(5):875-881. doi:10.1542/peds.101.5.875

60. Edinga-Melenge BE, Yakam AT, Nansseu JR, et al. Reference intervals for serum cystatin C and serum creatinine in an adult sub-Saharan African population. *BMC Clin Pathol*. 2019;19:4. doi:10.1186/s12907-019-0086-7

61. Cox J, Mann M. 1D and 2D annotation enrichment: a statistical method integrating quantitative proteomics with complementary high-throughput data. *BMC Bioinformatics*. 2012;13(16):S12. doi:10.1186/1471-2105-13-S16-S12

62. Oberbauer R, Rohrmoser M, Regele H, Mühlbacher F, Mayer G. Apoptosis of tubular epithelial cells in donor kidney biopsies predicts early renal allograft function. *J Am Soc Nephrol*. 1999;10(9):2006-2013. doi:10.1681/ASN.V1092006

63. Heyman SN, Rosenberger C, Rosen S. Experimental ischemia-reperfusion: biases and myths-the proximal vs. distal hypoxic tubular injury debate revisited. *Kidney Int*. 2010;77(1):9-16. doi:10.1038/ki.2009.347

64. Gobe GC, Johnson DW. Distal tubular epithelial cells of the kidney: Potential support for proximal tubular cell survival after renal injury. *Int J Biochem Cell Biol*. 2007;39(9):1551-1561. doi:10.1016/j.biocel.2007.04.025

65. The EMPA-KIDNEY Collaborative Group, Herrington WG, Staplin N, et al. Empagliflozin in Patients with Chronic Kidney Disease. *N Engl J Med*. 2023;388(2):117-127. doi:10.1056/NEJMoa2204233

66. Horvath S, Raj K. DNA methylation-based biomarkers and the epigenetic clock theory of ageing. *Nat Rev Genet*. 2018;19(6):371-384. doi:10.1038/s41576-018-0004-3

67. Meier F, Brunner AD, Frank M, et al. diaPASEF: parallel accumulation–serial fragmentation combined with data-independent acquisition. *Nat Methods*. 2020;17(12):1229-1236. doi:10.1038/s41592-020-00998-0

68. Perez-Riverol Y, Csordas A, Bai J, et al. The PRIDE database and related tools and resources in 2019: improving support for quantification data. *Nucleic Acids Res*. 2019;47(D1):D442-D450. doi:10.1093/nar/gky1106

ACKNOWLEDGMENTS

We thank the UK QUOD Consortium and NHS Blood and Transplant UK Registry for providing the samples and the associated clinical and demographic metadata. ; in particular we thank Sheba Ziyenge, Lewis Simmonds and Dr Sarah Cross, Dr Sergei Maslau and Mr Tomas Surik for their support on the QUOD sample selection.

We thank members of the Discovery Proteomics Facility within the TDI Mass Spectrometry Laboratory for expert help with mass spectrometry analysis, and members of the Lindgren group at the BDI for informative discussions regarding statistical modelling.

FIGURES AND TABLES

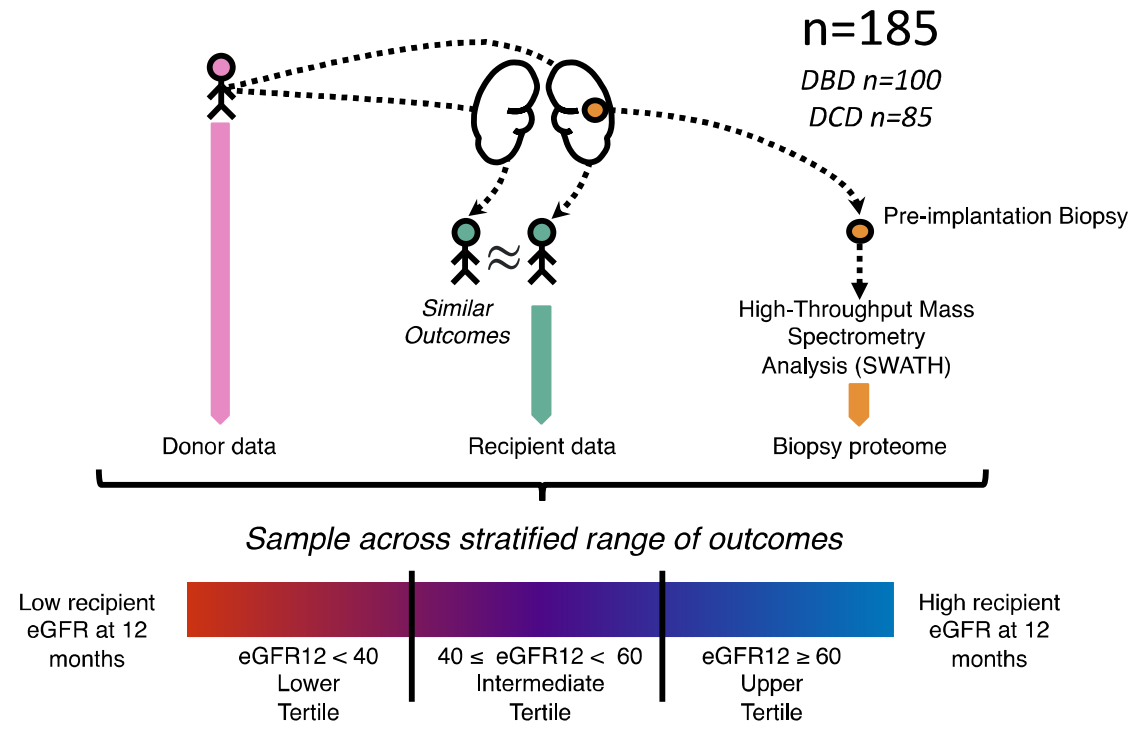

Figure 1: Experimental design to discover donor kidney proteome associations with transplant outcome
We selected biopsies from QUOD biobank taken from one kidney from each donor pair. Donor kidney samples were selected randomly from pairs where both recipients had similar outcomes. The biopsy samples were subjected to proteomic analysis to yield a snapshot of the organ proteome at kidney retrieval. We analyzed donor characteristics and clinical variables and protein abundances in a combined model against recipient eGFR at 12 months posttransplant (eGFR12; units given in ml/min/1.73 m^2).

Donor Type	**DBD**			**DCD**		
12m Outcome Tertile *ml/min/1.73 m²*	Lower *eGFR<40*	Intermediate *40≤eGFR<60*	Upper *eGFR≥60*	Lower *eGFR<40*	Intermediate *40≤eGFR≤60*	Upper *eGFR≥60*
n	31	31	38	31	28	26
Donor Age, y	56.84 ± 12.29	51.32 ± 12.24	39.05 ± 14.12	55.48 ± 9.34	53.57 ± 9.75	38.31 ± 12.28
Donor Sex						
Male	15 (48.4%)	16 (51.6%)	19 (50.0%)	22 (71.0%)	16 (57.1%)	16 (61.5%)
Female	16 (51.6%)	15 (48.4%)	19 (50.0%)	9 (29.0%)	12 (42.9%)	10 (38.5%)
Donor Ethnicity						
White	30 (96.8%)	30 (96.8%)	36 (94.7%)	30 (96.8%)	28 (100.0%)	25 (96.2%)
Other	1 (3.2%)	1 (3.2%)	2 (5.3%)	1 (3.2%)	0 (0.0%)	1 (3.8%)
Donor Weight, kg	82.53 ± 18.20	76.61 ± 18.07	81.38 ± 17.72	80.58 ± 14.95	82.43 ± 17.20	78.67 ± 13.96
Donor Height, cm	168.42 ± 9.37	169.52 ± 7.67	174.82 ± 11.16	169.97 ± 7.98	171.64 ± 9.73	174.65 ± 8.98
Donor S-Cr terminal, µmol/l	86.54 ± 40.81	82.57 ± 49.65	90.19 ± 67.36	73.37 ± 19.03	70.31 ± 39.02	59.60 ± 22.39
Donor CIT, h	15.80 ± 3.88	14.20 ± 4.60	13.42 ± 4.67	13.65 ± 5.20	11.72 ± 3.55	12.80 ± 4.49
Donor COD						
Trauma	1 (3.2%)	3 (9.7%)	3 (7.9%)	4 (12.9%)	3 (10.7%)	4 (15.4%)
Other	30 (96.8%)	28 (90.3%)	35 (92.1%)	27 (87.1%)	25 (89.3%)	22 (84.6%)
Donor UKKDRI	1.41 ± 0.52	1.10 ± 0.36	0.85 ± 0.36	1.31 ± 0.37	1.21 ± 0.40	0.73 ± 0.35
Recipient Age, y	53.03 ± 12.21	52.10 ± 14.61	39.71 ± 16.03	51.90 ± 9.85	50.93 ± 11.04	44.92 ± 12.87
Recipient Sex						
Female	15 (48.4%)	8 (25.8%)	12 (31.6%)	11 (35.5%)	9 (32.1%)	5 (19.2%)
Male	16 (51.6%)	23 (74.2%)	26 (68.4%)	20 (64.5%)	19 (67.9%)	21 (80.8%)
Recipient Ethnicity						
White	24 (77.4%)	21 (67.7%)	29 (76.3%)	22 (71.0%)	23 (82.1%)	20 (76.9%)
Other	7 (22.6%)	10 (32.3%)	9 (23.7%)	9 (29.0%)	5 (17.9%)	6 (23.1%)
Recipient Posttransplant Kidney Function (mean eGFR, ml/min/1.73 m²)						
3 months	29.71 ± 12.06	50.32 ± 17.28	78.54 ± 25.97	31.72 ± 12.24	46.50 ± 10.34	77.88 ± 18.57
12 months	26.58 ± 11.98	49.58 ± 6.10	85.58 ± 35.84	25.10 ± 12.01	48.24 ± 6.29	80.26 ± 15.91
HLA Mismatch Groups						
0 Mismatches	3 (10.0%)	4 (11.4%)	9 (25.7%)	1 (2.9%)	1 (4.2%)	0 (0.0%)
0 DR and 0/1 B	7 (23.3%)	13 (37.1%)	10 (28.6%)	10 (28.6%)	6 (25.0%)	8 (30.8%)
0 DR and 2 B or 1 DR and 0/1 B	17 (56.7%)	14 (40.0%)	13 (37.1%)	21 (60.0%)	14 (58.3%)	14 (53.8%)
1 DR and 2 B or 2 DR	3 (10.0%)	4 (11.4%)	3 (8.6%)	3 (8.6%)	3 (12.5%)	4 (15.4%)

831 **Table 1: Donor and recipient clinical and demographic variables**
832 Donor kidney associated metadata. Samples are subdivided by donor type and by final assigned outcome tertile.
833 Numerical variables are given ± standard deviation. Categorial variables are given alongside percentage of total
834 cohort

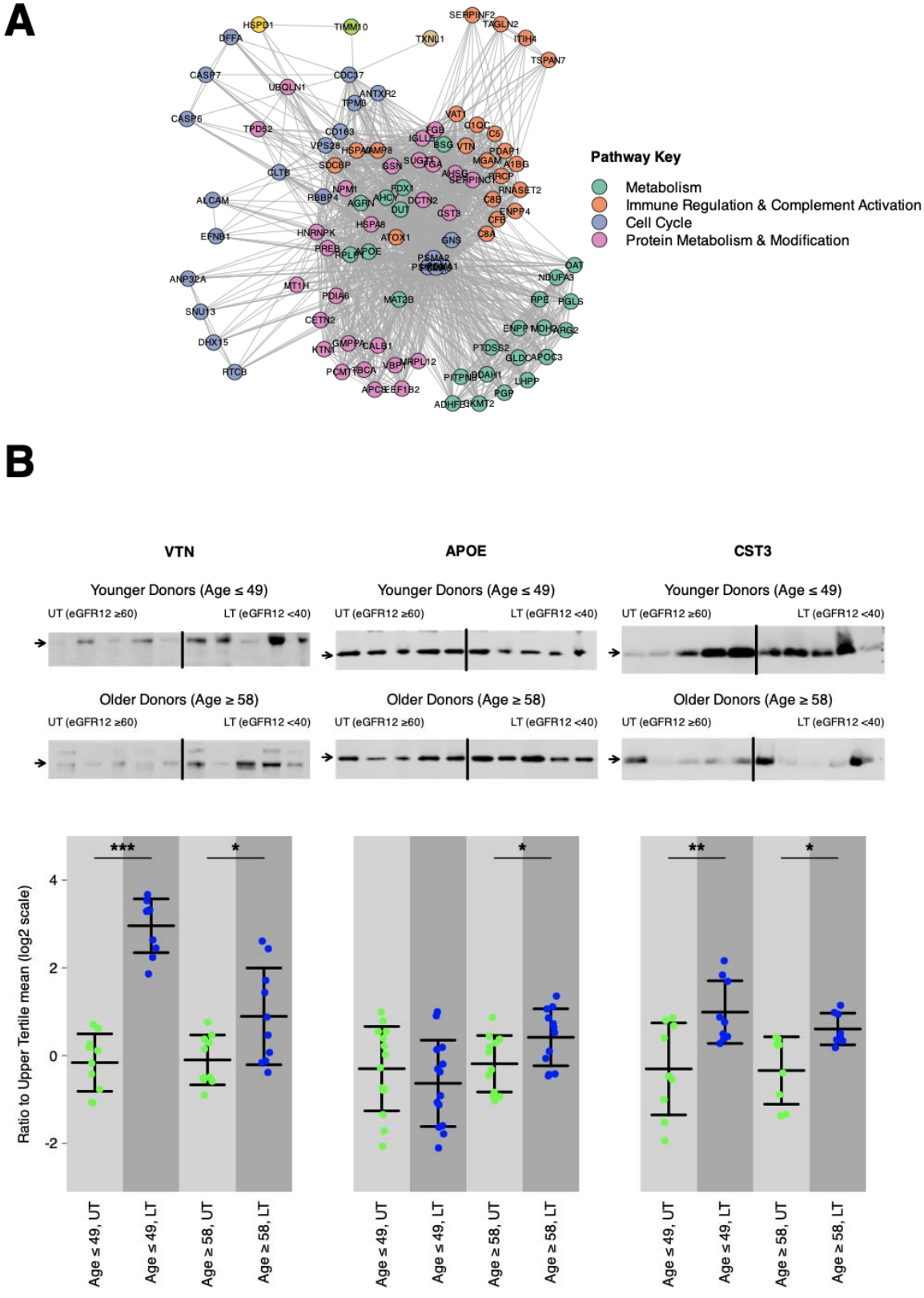

Figure 2: Proteins predicting transplant outcome show immuno-metabolic functional associations, predict low eGFR outcomes and are consistent with Western Blot assay results.

A: Shared Reactome pathway membership network analysis of filtered features. Nodes are colored by assigned cluster, and the clusters are annotated according to the top three most enriched pathways within each cluster.

B: Western blots comparing younger (age $\leq$ 49; mean age 34) and older (age $\geq$ 58; mean age 64) donors between Upper Tertile (UT; eGFR12 $\geq$ 60) and Lower Tertile (LT; eGFR12 < 40) outcomes. As above, Left-Right: VTN, APOE, CST3. Top row: representative western blots (n=5 per group) from comparison of younger donors. Middle row: representative western blots (n=5 per group) from comparison of older donors. Bottom row: result values for all quantified samples relative to the UT mean. UT values in green, LT values in blue. Error bars indicate ±1 standard deviation; the central wider bar indicates mean. Significance stars indicate t-test comparison p-values (***: $p < 0.001$, *: $p < 0.05$).

All eGFR12 units given in ml/min/1.73 m^2

Cluster Label	Top 3 Shared Pathways
Immune Regulation & Complement Activation	Immune System Innate Immune System Regulation of Complement Cascade
Protein Metabolism and Regulation	Metabolism of Proteins Post-translational Protein Modification Post-translational Protein Phosphorylation
Metabolism	Metabolism Metabolism of Amino Acids and Derivatives Retinoid Metabolism and Transport
Cell Cycle	Cyclin E Associated Events During G1/S Transition Cyclin A:Cdk2-associated Events at S Phase Entry PCP/CE Pathway

Table 2: Major Shared Pathway Network Clusters
Proteins in Figure 2A were clustered by pathway membership, forming 4 major clusters (those with more than a single member). We assigned summary labels to each cluster based on the top 3 pathways with shared membership in each cluster.

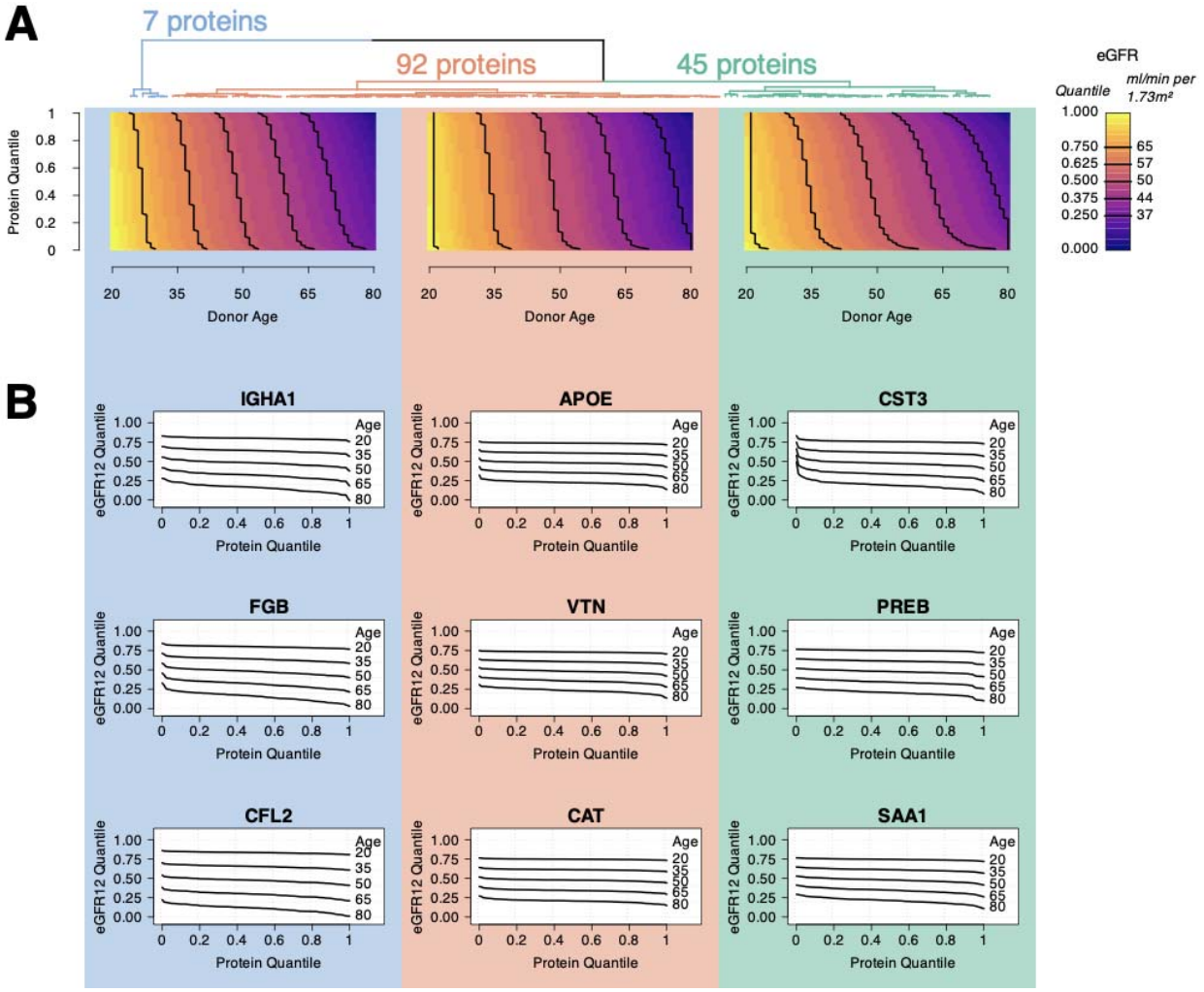

Figure 3: Modelled associations between proteins and kidney transplant outcome change with donor age
Our modelling found that the effect of candidate protein levels on outcome changed with age.
A: We quantile-normalized protein levels to a consistent scale and predicted outcome (12-month posttransplant eGFR) across a representative donor age range. Using this prediction matrix to compare the interaction with age between protein models, we found 3 major clusters (Left-Right; blue, pink and green dendrogram branches and corresponding plot background color) representing increasing levels of age modulation. Moving Left-Right across each plot, the eGFR12 (color scale, see key on right) contours across protein quantile (y axis) change as donor age (x axis) increases.
B: Illustrative protein quantile-GFR12 plots are shown for each three proteins in each cluster. Traces are shown for donor ages between 20 and 80 as labelled on the right end of each trace.

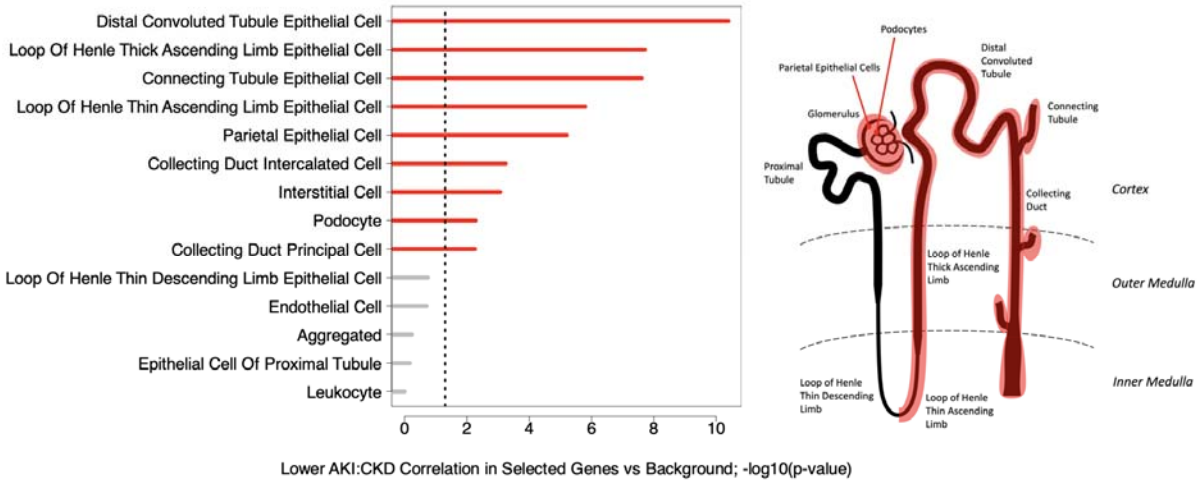

Figure 4: Independent scRNA-seq Data Indicate Spatial Localization of the Outcome-Associated Signature
We reasoned that proteins/genes which predict outcome should associate with specific facets of organ injury rather than general inflammatory and stress response, and therefore would be expected to have a *lower* expression correlation between acute and chronic damage scenarios than non-predictive other proteins/genes. We explored this in a spatially resolved public transcriptomic dataset and found that the degree of correlation was significantly lower for the set of 144 candidate predictors identified by our modelling approach, but that the signal appears to be spatially localized, primarily to distal convoluted tubule epithelial cells and the epithelia of neighboring tubules (indicated by red highlighting in right hand diagram).